THE JOURNAL OF BIOLOGICAL CHEMISTRY VOL. 292, NO. 10, pp. 4293–4301, March 10, 2017

Na^+/H^+ Exchanger 9 Regulates Iron Mobilization at the Blood-Brain Barrier in Response to Iron Starvation*

Received for publication, November 22, 2016, and in revised form, January 24, 2017 Published, JBC Papers in Press, January 27, 2017, DOI 10.1074/jbc.M116.769240

Rami Beydoun[1], **Mohamed A. Hamood**[1], **Daniela M. Gomez Zubieta, and Kalyan C. Kondapalli**[2]
From the Department of Natural Sciences, University of Michigan-Dearborn, Dearborn, Michigan 48128

Edited by Paul E. Fraser

Iron is essential for brain function, with loss of iron homeostasis in the brain linked to neurological diseases ranging from rare syndromes to more common disorders, such as Parkinson's and Alzheimer's diseases. Iron entry into the brain is regulated by the blood-brain barrier (BBB). Molecular mechanisms regulating this transport are poorly understood. Using an *in vitro* model of the BBB, we identify NHE9, an endosomal cation/proton exchanger, as a novel regulator of this system. Human brain microvascular endothelial cells (hBMVECs) that constitute the BBB receive brain iron status information via paracrine signals from ensheathing astrocytes. In hBMVECs, we show that NHE9 expression is up-regulated very early in a physiological response invoked by paracrine signals from iron-starved astrocytes. Ectopic expression of NHE9 in hBMVECs without external cues induced up-regulation of the transferrin receptor (TfR) and down-regulation of ferritin, leading to an increase in iron uptake. Mechanistically, we demonstrate that NHE9 localizes to recycling endosomes in hBMVECs where it raises the endosomal pH. The ensuing alkalization of the endosomal lumen increased translocation of TfRs to the hBMVEC membrane. TfRs on the membrane were previously shown to facilitate both recycling-dependent and -independent iron uptake. We propose that NHE9 regulates TfR-dependent, recycling-independent iron uptake in hBMVECs by fine-tuning the endosomal pH in response to paracrine signals and is therefore an important regulator in iron mobilization pathway at the BBB.

There is high demand for iron in the brain, one of the most metabolically active organs in the body (1, 2). Iron is a co-factor of several proteins involved in specialized brain cell functions such as synthesis of neurotransmitters and myelination (3–5). Iron is also necessary for housekeeping functions such as mitochondrial respiration and DNA synthesis, crucial for brain function (5). Insufficient or surplus iron in the brain has been associated with various neurological diseases (6–10). Although iron deficiency is associated with cognitive and brain structural deficits, excess brain iron is implicated in Alzheimer's, Parkinson's, and other neurodegenerative diseases (10, 11). Therefore, it is not surprising that iron levels are tightly regulated in the brain (10).

Iron entry into the brain is regulated by the blood-brain barrier (BBB)[3] (10). This physiological barrier is characterized by tight junctions between brain microvascular endothelial cells (BMVECs) that block passive diffusion of iron into the brain (12). BMVECs are polarized cells with one surface (apical) facing the blood and the other (basal or abluminal) facing interstitial fluid of the brain. BMVECs and ensheathing astrocytes form the regulatory axis of the BBB, modulating iron transport from blood into the brain interstitium (2, 13). It is now known that BMVECs are the focal point for regulation of cerebral iron homeostasis and not mere conduits for iron transport (14). Paracrine factors released by neighboring astrocytes communicate iron status of the brain to BMVECs (14, 15). *In vitro* studies have so far identified hepcidin, ceruloplasmin, interleukin-6, soluble amyloid precursor protein, and holo-transferrin as some of the candidates in astrocyte secretome that communicate iron status to BMVECs (14–16). Secretions from astroglial cells cultured in iron-deficient and -loaded media have been shown to differentially regulate the expression and distribution of the known iron transport protein transferrin receptor in BMVECs (14). The dynamics of brain iron uptake are far from understood. In view of the significant health implications, it is essential to examine the expression of iron transport proteins in BMVECs and evaluate their roles in iron uptake. In this report, we provide experimental evidence that identifies NHE9 as member of the iron regulatory network at the BBB.

NHE9 belongs to a subfamily of endosomal $\underline{Na}^+(K^+)/\underline{H}^+$ Exchangers that shuttle K^+ or Na^+ from the cytoplasm into endosomes in exchange for H^+ (17–19). Mutations and gene expression changes in SLC9A9, gene coding for NHE9, underlie neurological diseases with distinct clinical phenotypes (20–26). Loss and gain of NHE9 function have been associated with human disease (26–28). Overexpression of NHE9 causes excess leak of protons from the recycling endosomes resulting in more alkaline endosomes (28). In glioblastoma multiforme, increased alkalization of endosomes has been shown to exert post-translational control of EGF receptor turnover and consequently increased persistence of oncogenic signaling pathways

* This work was supported by funds provided to Kalyan C. Kondapalli by the Department of Natural Sciences and Office of Research and Sponsored Programs, University of Michigan-Dearborn. The authors declare that they have no conflicts of interest with the contents of this article.
[1] Both authors contributed equally to this work.
[2] To whom correspondence should be addressed: Dept. of Natural Sciences, University of Michigan-Dearborn, 4901 Evergreen Rd., ASC #207, Dearborn, MI 48128. E-mail: kondap@umich.edu.

[3] The abbreviations used are: BBB, blood-brain barrier; BMVEC, brain microvascular endothelial cell; hBMVEC, human brain microvascular endothelial cell; TfR, transferrin receptor; TEER, transendothelial electrical resistance; ZO1, zona occludens 1; FHC, ferritin heavy chain; LBPA, lysobisphosphatidic acid; IRP, iron regulatory protein; LIP, labile iron pool; DMT1, divalent metal ion transporter 1; qPCR, quantitative PCR.

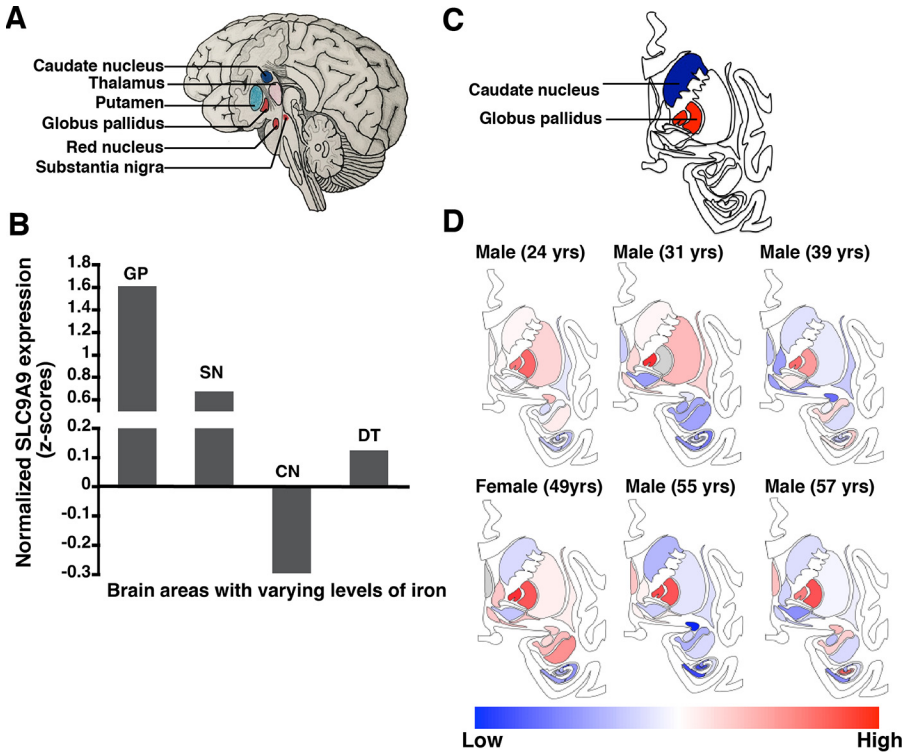

FIGURE 1. **NHE9 is highly expressed in regions of the brain with high iron content.** *A*, schematic representation of the brain highlighting regions of varying iron concentrations. Color representation is according to a *blue-red* heat map shown at the *bottom* of the figure (relatively low iron regions, *blue*; relatively high iron regions, *red*). *B*, normalized expression (*z* scores) levels of NHE9 in regions of the adult human brain with relatively high (globus pallidus (*GP*) and substantia nigra (*SN*)) and low (caudate nucleus (*CN*) and dorsal thalamus (*DT*)) iron content, determined from microarray data obtained from Allen Brain Atlas. *C*, schematic of subcortical structures of the brain represented from a frontal view highlighting regions of the adult human brain with highest (*red*) and lowest (*blue*) iron content. *D*, anatomical abstract view of NHE9 expression pattern of each donor brain used for microarray analysis, obtained from Allen Brain Atlas. Subcortical structures represented from a frontal view with *blue-red* heat map to visualize microarray data. The colors of the heat map represent normalized expression values. *Blue color* in the heat map represents relatively low NHE9 expression, and *red* represents relatively high NHE9 expression. The color heat map scale is shown at the *bottom* for reference.

(28). On the other hand, loss of NHE9 exchanger function as a result of mutations in SLC9A9 leads to hyperacidification of sorting endosomes (27). Functional evaluation of these autism-associated mutations in astrocytes showed that these cells lose their ability to clear glutamate to a significant extent as a consequence of dysregulated trafficking of glutamate transporter (GLAST) (27). Moreover, global knock-out SLC9A9 mice (*Slc9a9* KO) show traits of autism spectrum and attention deficit hyperactivity disorder (29). Thus, by modulating endosomal pH, NHE9 could regulate delivery and recycling of various endocytic cargos, including proteins involved in iron homeostasis. Consistent with this, genome-wide association studies have recently been identified NHE9 as risk factor in Alzheimer's disease (30). Single nucleotide polymorphisms in SLC9A9 have been associated with late onset Alzheimer's disease (31, 32). More recently, significant association between NHE9 variants and Alzheimer's disease was identified in meta-analysis of a large genome-wide association study data set that included 5000 individuals (33).

To investigate the role of NHE9 in iron mobilization, we used an *in vitro* model BBB system. We examined the regulation of NHE9 and transferrin receptor expression in human brain microvasculature cell line (hBMVECs) by paracrine factors from C6 glial cells conditioned in iron-deficient and -loaded media. Next, we selectively manipulated the expression of NHE9 in hBMVECs to mimic the response to iron requirement signals and investigated the mechanistic basis for role of NHE9 in iron uptake.

Results

NHE9 Expression Correlates with Iron Distribution in Adult Human Brain—Iron concentrations in the human brain vary both temporally and spatially (34). Perls staining and MRI studies on distribution of iron in the brain suggest that large amounts of iron are sequestered in globus pallidus, substantia nigra, and red nucleus in the midbrain relative to other regions such as the putamen, caudate nucleus, and the dorsal thalmus (35–37). Proteins that comprise the iron regulatory network could contribute to the changes in brain iron concentrations (36). In this context, we evaluated the expression of NHE9 in iron-rich and -poor regions of the brain (Fig. 1*A*). Microarray analysis of adult human brain tissue ($n = 6$ postmortem brains) obtained from the Allen Brain Atlas (38) indicates that the expression levels of NHE9 are higher in globus pallidus (zero score normalization = 1.61) and substantia nigra (zero score normalization = 0.67) compared with caudate (zero score normalization = −0.29) and the dorsal thalmus (zero score normalization = 0.12) (Fig. 1, *B–D*). High densities of iron transport and storage proteins are found in iron-rich areas of the brain or in regions that connect to them (36). For example, although ferritin is expressed in iron-rich regions, high transferrin receptor (TfR) expression is observed in brain regions

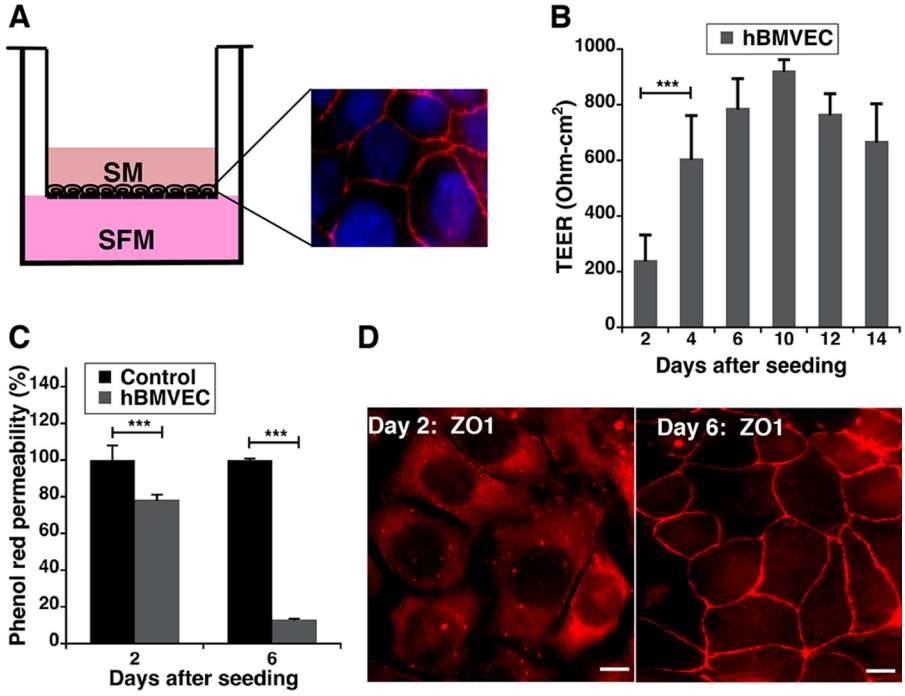

FIGURE 2. **Validating an *in vitro* model BBB system.** *A*, BBB was mimicked *in vitro* using a Transwell culture system. hBMVECs were seeded on Transwell filters, with serum in the upper chamber (serum medium (*SM*)) to represent the apical side facing the blood and without serum in the lower chamber (serum-free medium (*SFM*)) to represent the basal side facing brain interstitial fluid. The *inset* shows hBMVECs with characteristic tight junctions between endothelial cells (indirect immunofluorescence image, *red*; tight junction marker ZO1, *blue*: DAPI staining). *B*, transendothelial electrical resistance values for hBMVECs grown in Transwell model system for 2 weeks. *C*, diffusive permeability of the *in vitro* BBB model to phenol red. *D*, indirect immunofluorescence images of hBMVECs ZO1. *Scale bars*, 10 μm. The *error bars* represent S.D. determined from at least three biological replicates; ***, $p < 0.001$. Statistical analysis was done using Student's *t* test.

that connect with globus pallidus and substantia nigra (10, 37). This could possibly indicate the need for iron uptake from one area and delivery via axonal transport for functional or storage purpose in iron-rich regions of the brain (36). Similar to these iron homeostasis proteins, NHE9 expression in globus pallidus and substantia nigra is 3.32-fold ($p = 1.09 \times 10^{-29}$) and 2.50-fold ($p = 9 \times 10^{-16}$) higher than in the caudate nucleus, respectively. These data support the idea of a role for NHE9 in brain iron homeostasis.

Glial Cell Conditioned Medium Stimulates NHE9 Expression in hBMVECs—Glia ensheath endothelial cells on their basal surface (2, 13). Paracrine factors released by glia are known to regulate the expression of iron homeostasis proteins in endothelial cells (14, 15). We used a Transwell system to mimic the BBB *in vitro* to test the effect of iron-conditioned glial cell medium on NHE9 expression in hBMVECs (14, 15, 39). This cell line is commonly used in BBB models (15, 40, 41). hBMVECs are polarized, with their apical surface facing the blood and their basal surface facing the brain parenchyma. The upper chambers of the Transwells are filled with medium containing serum to mirror the capillary milieu, whereas the lower chamber contained medium without serum to mirror the brain interstitium (Fig. 2*A*). Intercellular tight junctions are a characteristic feature of endothelial cells found in the blood-brain barrier (10, 12). We used three different approaches to measure tight junction integrity of hBMVECs growing on the upper surface of the Transwell membrane (Fig. 2, *B–D*). hBMVECs formed tight junctions after 5–6 days as demonstrated quantitatively via transendothelial electrical resistance (TEER) and phenol red diffusion assays (Fig. 2, *B* and *C*). We also used immunofluorescence microscopy to detect the tight junction marker zona occludens 1 (ZO1). Consistent with our BBB model, the cells imaged on day 6 showed increased presence of ZO1 on membrane junctions of hBMVECs compared with day 2 (Fig. 2*D*). Next, we cultured C6 glioma cells, a commonly used astrocytic model in co-cultures with BMVECs (15, 42–44), in iron-conditioned medium (Fig. 3*A*). In hBMVECs, within 2 h of exposure to medium from iron-deficient astrocytes, NHE9 mRNA increased by ~5-fold relative to control (Fig. 3*B*). In 24 h, we observed a ~19-fold increase in NHE9 transcript levels (Fig. 3*B*). Consistent with previous observations (14), TfR expression was enhanced by 19-fold (Fig. 3*B*). However, unlike NHE9, there was no significant change in TfR expression within the first 2 h of exposure (Fig. 3*B*). Medium from iron-loaded astrocytes altered NHE9 expression; however, under our test conditions, the variation failed to achieve statistical significance (Fig. 3*C*). TfR expression, however, decreased significantly (Fig. 3*C*). These data indicate that NHE9 is regulated early in the physiological response invoked by iron-deficient astrocytes to mobilize iron. Based on these data, it is also possible that NHE9 could be co-regulated with TfR in the iron transport pathway at the BBB.

NHE9 Expression in hBMVECs Activates Iron Starvation Response to Promote Iron Uptake—Next, we evaluated the hBMVECs response to an increase in NHE9 expression. However, instead of using paracrine signals from iron-deficient astrocytes as the stimulants, we engineered lentiviral-mediated expression of NHE9-GFP in hBMVECs. An increase in NHE9

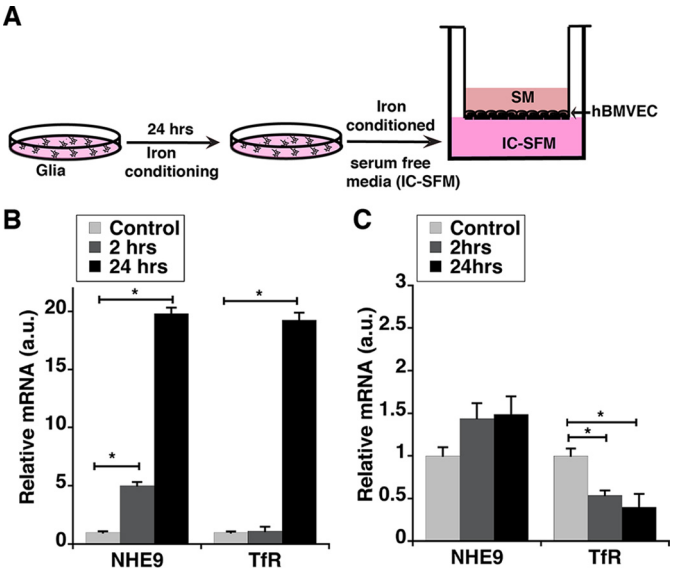

FIGURE 3. **Paracrine signals from iron-depleted glia up-regulate NHE9 expression in hBMVECs.** *A*, schematic representation of the iron-conditioning experiment as described under "Materials and Methods." *B*, qPCR analysis of NHE9 and TfR transcripts from hBMVECs cultured on Transwell filters, after 2 and 24 h of exposure to serum-free medium from iron-deficient or iron-sufficient (control) C6 glia. *C*, qPCR analysis of NHE9 and TfR transcripts from hBMVECs cultured on Transwell filters, after 2 and 24 h of exposure to serum-free medium from iron-loaded or iron-sufficient (control) C6 glia. The *error bars* represent S.D. determined from at least three biological replicates. *, $p < 0.05$. Statistical analysis was done using Student's *t* test.

expression would elicit a response despite the absence of astrocyte-directed starvation signals, if NHE9 is co-regulated or is acting upstream in the iron deprivation response pathway. To test this hypothesis, we overexpressed NHE9-GFP in hBMVECs grown on the upper surface of our Transwell system. The lower chamber contained medium from C6 cells cultured in iron-sufficient (control) medium. Transcript analysis by quantitative PCR revealed a 10-fold increase in NHE9 expression in hBMVECs (Fig. 4*A*). We also confirmed NHE9-GFP expression by immunofluorescence (Fig. 4*B*). In response to iron starvation, mammalian cells are known to decrease the levels of iron storage protein, ferritin, and increase TfR expression, ultimately resulting in iron uptake (14, 45). Hence, we evaluated ferritin and TfR expression by Western blotting analysis. We observed a 2.5-fold decrease in ferritin heavy chain (FHC) protein, whereas TfR expression increased by 2-fold, in hBMVECs overexpressing NHE9 relative to control cells (Fig. 4, *C–E*). These data support our hypothesis that NHE9 is co-regulated or is acting upstream in the iron starvation response pathway. Following this, we used atomic absorption spectroscopy to measure total cellular iron levels in hBMVECs 72 h after lentiviral transduction of NHE9-GFP. Consistent with activation of the pathway, we observed a ~1.5-fold increase in total cellular iron in NHE9 overexpressing hBMVECs relative to control cells (Fig. 4*F*).

NHE9 Localizes to Early and Recycling Endosomes and Regulates Endosomal pH in hBMVECs—To determine the mechanistic basis of increase in iron uptake with NHE9 expression, we first studied the subcellular localization of NHE9-GFP in hBMVECs. NHE9-GFP co-localized partially with markers for the early endosome Rab 5 (Manders' coefficient, 0.39 ± 0.04 S.D., $n = 30$) and more extensively with the recycling endosome marker Rab11 (0.61 ± 0.07 S.D., $n = 40$) by immunofluorescence microscopy (Fig. 5*A*, *top* and *middle panels*). NHE9-GFP co-localized with lysobisphosphatidic acid (LBPA) (0.09 ± 0.02 S.D., $n = 40$; Fig. 5*A*, *bottom panels*) in the late endosome although to a much lesser extent than early and recycling endosomes. These results are consistent with NHE9 localization observed in other cell models (27, 46). The endosomal lumen is acidified by the V-ATPase (17). NHE9 transports these protons out in exchange for sodium or potassium ions (19, 20, 47). Therefore, an increase in NHE9 expression caused by iron deprivation signals would result in more alkaline endosomal lumen relative to control. Luminal pH of the endosome (pH_e) was measured using pH-sensitive fluorescence of FITC-tagged transferrin. pH_e was calibrated using buffers of known pH (Fig. 6*A*). In hBMVECs, we observed pH_e change from 5.62 ± 0.14 to 6.51 ± 0.37 (Fig. 6*B*) with lentivirus-mediated expression of NHE9.

NHE9 Controls Trafficking of Transferrin Receptors—Endosomal pH is critical for turnover of plasma membrane proteins (27, 28). Transferrin-bound iron is a major contributor to hBMVECs total cellular iron (2, 14, 48). Therefore, we investigated whether the increase in iron uptake observed in hBMVECs expressing higher levels of NHE9 is a result of altering the turnover of the TfRs. We used two complementary approaches to address this. First, we used biotinylation of cell surface proteins followed by Western blotting analysis to quantitatively compare TfR densities on the plasma membrane. However, based on our previous experiments, we knew that there is an increase in TfR expression in hBMVECs with an increase in NHE9 expression. We normalized surface TfR levels to total TfR expression in the cells to account for differences in cellular protein expression. NHE9 expression in hBMVECs increased surface levels TfR by ~3-fold (Fig. 7, *A* and *B*). Next, we compared the effect of NHE9 overexpression on the rate of transferrin efflux as a method to evaluate TfR turnover at the plasma membrane. After loading the cells in serum-free medium with fluorescently tagged transferrin (Tfn-568) for 30 min, we monitored the efflux of Tfn-568 by incubating the cells in medium with serum for 10 min. hBMVECs expressing NHE9-GFP exported ~49.1 ± 2.58% of Tfn-568 in the first 10 min compared with ~ 28.26 ± 1.6% in control (Fig. 7, *C* and *D*). These data along with the surface biotinylation data confirmed our hypothesis that NHE9 expression in hBMVECs regulates the turnover of TfR to affect iron uptake.

Discussion

Astrocytes are situated optimally to function as iron sensors for the brain and to communicate brain iron needs to the BBB via paracrine signaling (7, 13, 14). Here, we show that the physiological response invoked by iron-deficient astrocytes includes elevation of total iron levels in human brain microvascular endothelial cells. Recently, other groups have addressed paracrine signal-dependent release of iron from endothelial cells via ferroportin (14, 15). However, iron acquisition by hBMVECs as a part of this response has not been investigated. Our data in context of the existing paradigm suggest that iron mobilization across the BBB appears to be at least a two-step process,

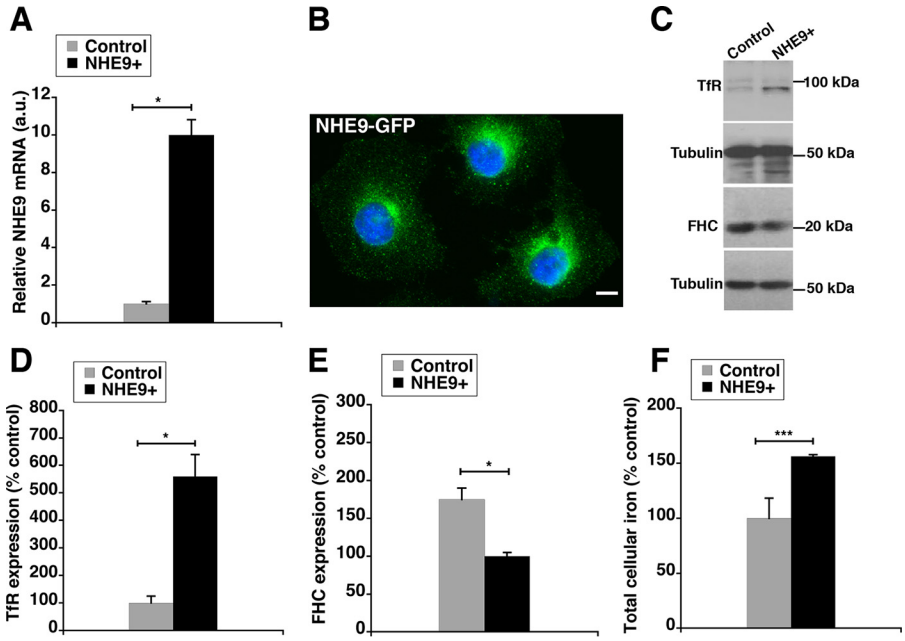

FIGURE 4. **NHE9 expression activates iron starvation response in hBMVECs.** *A*, qPCR analysis showing the efficacy of expression of NHE9-GFP in hBMVECs. The data are plotted as average fold changes of mRNA levels relative to control. The *error bars* represent S.D. determined from at least three biological replicates. *, $p < 0.05$. Statistical analysis was done using Student's *t* test. *B*, NHE9-GFP expression in hBMVECs determined by immunofluorescence microscopy after fixing with 3.7% paraformaldehyde. *C*, expression levels of TfR and FHC proteins in hBMVECs expressing NHE9-GFP and control cells. Immunoblots of hBMVECs lysate used anti-TfR, anti-FHC, and anti-tubulin antibodies. *D* and *E*, graphs represent average band intensity from densitometric scans of immunoblots from three biological replicates. TfR and FHC levels were normalized to tubulin and shown relative to control. The *error bars* represent S.D. *, $p < 0.05$. Statistical analysis was done using Student's *t* test. *F*, intracellular iron concentrations measured by atomic absorption spectroscopy and normalized to total cellular protein. The graph represents an average of six biological replicates and is shown relative to control. The *error bars* represent S.D. ***, $p < 0.001$. Statistical analysis was done using Student's *t* test.

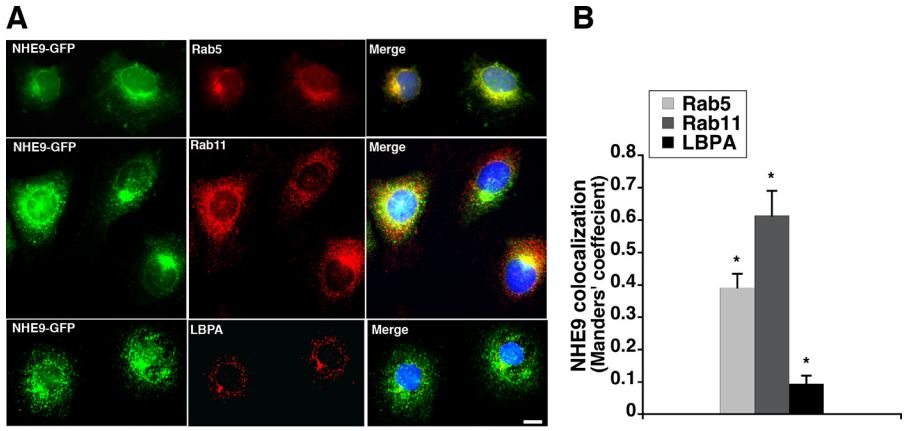

FIGURE 5. **NHE9 localizes to recycling endosomes in hBMVECs.** *A*, subcellular localization of NHE9-GFP in hBMVECs determined by immunofluorescence microscopy. *Top panel*, NHE9-GFP (*green*) and early endosome marker, Rab5 (*red*). *Middle panel*, NHE9-GFP (*green*) and recycling endosome marker Rab11 (*red*). *Bottom panel*, NHE9-GFP (*green*) and late endosome marker LBPA (*red*). Co-localization is indicated by *yellow* in the *merge*. *Blue* represents DAPI staining in all images. The *scale bar* is 10 μm. *B*, quantification of NHE9-GFP localization with the indicated organellar markers in hBMVECs using Manders' coefficient. At least 30 cells were used for quantification for each marker. The *error bars* represent S.E. *, $p < 0.05$. Statistical analysis was done using Student's *t* test.

invoked by iron requirement signals released by astrocytes. Whether the release of iron from the endothelial cells happens first followed by iron uptake to replace the released iron or vice versa is yet to be determined. In the former case, iron release from the endothelial cells could trigger the iron regulatory protein (IRP) function to stabilize mRNA of iron uptake proteins. Although NHE9 transcript has revealed no IRP binding sequence, IRP function is known to stabilize transferrin receptor when intracellular iron status is low. Consistent with this, Connor *et al.* (49) showed IRP1 mRNA expression in brain microvasculature. Investigations into how NHE9 is regulated are currently underway and could provide new insight into paracrine signal-based regulation for iron mobilization across the BBB.

Cytosolic labile iron pool (LIP) is a principal metabolic source of metal to hBMVECs, and transferrin-mediated iron uptake is a major contributor to LIP (50). hBMVECs receive Fe^{3+} from circulation bound to transferrin (holo-transferrin). Receptor-mediated endocytosis of holo-transferrin is the canonical physiological mode of iron delivery to cells (2). Electrochemical potential (E^0) of transferrin iron complex is too negative, and acidification of endosomal lumen has been sug-

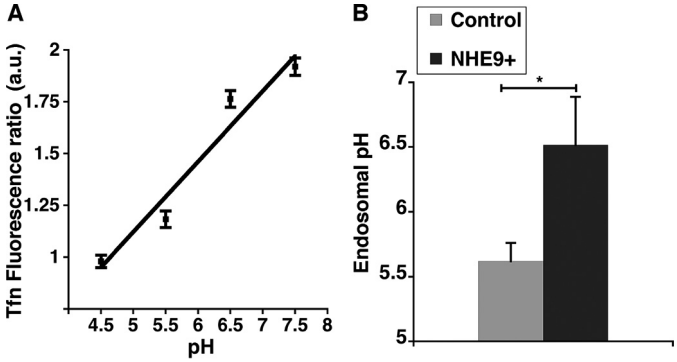

FIGURE 6. **NHE9 expression makes the endosomes more alkaline.** *A*, calibration of endosomal pH in hBMVECs. *B*, pH in endosomal compartments is alkalinized in hBMVECs overexpressing NHE9 relative to control. Graph represents means from three biological replicates, and at least 50 cells were used for pH quantification in each experiment. The *error bars* represent S.D. *, $p < 0.05$. Statistical analysis was done using Student's *t* test.

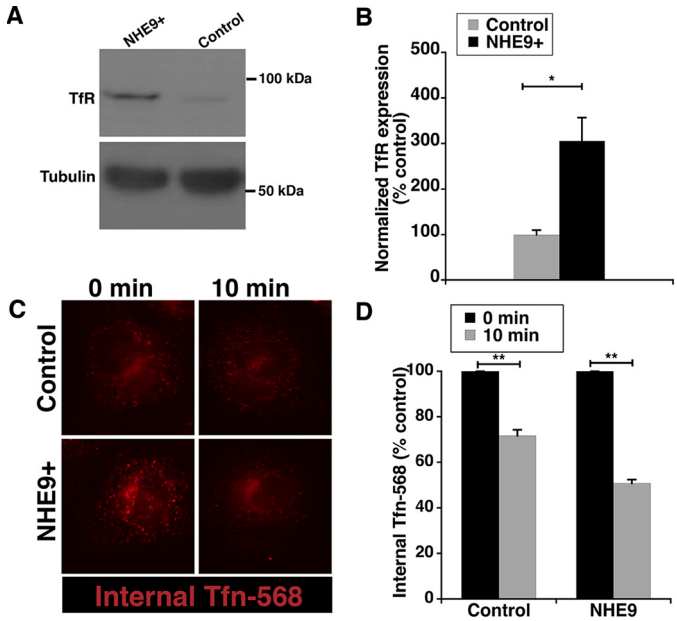

FIGURE 7. **Trafficking of transferrin receptors to hBMVECs plasma membrane is regulated by NHE9.** *A*, immunoblot of TfR from plasma membranes obtained by surface biotinylation of hBMVECs control and NHE9-GFP expressing cells. *B*, graph represents average band intensity from densitometric scans of immunoblots after surface biotinylation from three biological replicates, normalized to total TfR protein levels. The *error bars* represent S.D. *, $p < 0.05$. Statistical analysis was done using Student's *t* test. *C*, efflux of Alexa Fluor 568-tagged transferrin (Tfn-568) was monitored by loss of fluorescence, after loading hBMVECs for 30 min in serum-free medium followed by incubation in medium with serum for 10 min. Representative images show Tfn-568 remaining in control and NHE9-GFP expressing hBMVECs after 0 and 10 min. *D*, plot represents mean fluorescence intensity of Tfn-568 remaining in hBMVECs, from three biological replicates. At least 30 cells were used for fluorescence quantification in each experiment. The *error bars* represent S.D. **, $p < 0.01$. Statistical analysis was done using Student's *t* test.

gested to make the E^0 more positive (29). Thus, a drop in the pH caused by proton influx via V-ATPase in the sorting endosomes could lead to release of iron from holo-transferrin-TfR complex. Divalent metal ion transporter 1 (DMT1) is the only divalent cation transporter to have been identified in brain microvascular endothelial cells and is thought to play a role in export of released iron from the endosomes to the cytosol (14, 48, 51). The function of DMT1 is again pH-dependent (52). We showed that an increase in expression of NHE9 leads to alkalinizing the endosomal lumen. Limiting acidification could negatively affect release of iron and export via DMT1 to the cytosol. Therefore, increasing the expression of NHE9 may not promote endosome-dependent, TfR-mediated iron uptake.

Reduction of Fe^{3+} and release from transferrin has now been shown to occur also at the cell surface and is associated with exo-cytoplasmic ferrireductases (48). However, efficient ferri-reduction at the cell surface is dependent on binding of holo-transferrin to TfR. Inhibition of cell surface reductase activity or binding of holo-transferrin to TfR significantly decrease ferri-reduction (48). Ferrous iron transporter on the plasma membrane has not been identified, but Zip1 has been proposed as a potential candidate (48). McCarthy and Kosman (48) showed that iron reduced from holo-transferrin bound to TfR at the cell surface accounts for at least 50% of the iron uptake observed in hBMVECs. This could explain up-regulation of NHE9 by hBMVECs, *i.e.* to increase membrane persistence of TfRs, thereby promoting reduction of iron and consequently iron uptake at the cell surface. Canonical uptake from iron released in the endosome may not make a quantitatively significant contribution to LIP in hBMVECs. However, we show that fine-tuning of endosomal pH by NHE9 is important for iron acquisition by hBMVECs. Our data clearly suggest that NHE9 responds to brain requirements for iron. In neurological diseases resulting from iron overload, it is possible that NHE9 activity could be selectively manipulated to therapeutically titrate brain iron levels. Multiple classes of drugs targeting various solute carrier transporters have already been developed, including inhibitors of another isoform from the NHE family, NHE1. Thus, insights gained from this and follow-up studies should potentially provide a new target for developing therapeutics against excessive brain iron accumulation.

Materials and Methods

Cell Culture and Plasmids—hBMVECs were obtained from Dr. Alfredo Quiñones-Hinojosa (Johns Hopkins University) (53). The generation and characteristics of this cell line have been described in detail (54). C6 glioma cells were obtained from Dr. Gregory Kapatos (Wayne State University) (55). hBMVECs and C6 glioma cells were maintained in M199 medium (Invitrogen) supplemented with 10% fetal bovine serum (Sigma) and 5% antibiotic-antimycotic (10,000 units/ml penicillin, 10,000 mg/ml streptomycin; Gibco). The cells were maintained in a 5% CO_2 incubator at 37 °C. The growth medium was completely exchanged with fresh medium twice a week. Full-length mNHE9-EGFP and mNHE9-mcherry were cloned into FuGW lentiviral vector as previously described (27). Empty vector (FuGW) was used for control transductions. The viral Core Facility of the University of Michigan executed lentiviral packaging of the virus.

In Vitro Model of the Blood-Brain Barrier—hBMVECs were cultured by seeding 300 μl of M199 growth medium containing 5×10^4 cells in the upper chamber and 1000 μl of growth medium in the lower chamber of a 24-well plate insert (Thincert, 0.4-micron transparent insert; USA Scientific) were grown to confluence for at least 5 days. TEER was monitored using EVOM volt-ohmmeter (World Precision Instruments, Sarasota, FL). The average TEER of the monolayers on days 5–6 was

$\sim$560 Ohm-cm^{-2} and did not change significantly thereafter. For some experiments, the permeability of hBMVECs monolayers was also evaluated by phenol red diffusion assay. M199 growth medium in the lower chamber was replaced by a similar medium without phenol red (1000 μl) and incubated for 2 h. The diffusion of phenol red across the monolayer was determined by measuring absorbance at 546 nm (56). Indirect immunofluorescence imaging of the tight junction marker ZO1 (Life Technologies) was also used to measure tight junction integrity as described below.

Iron-conditioned Media—C6 glioma cells were plated at 2×10^5 cells/ml and grown to confluence in a 24-well plate. The cells were treated with serum-free medium (control), serum-free medium with 100 μM deferoxamine (iron-deficient), or serum-free medium with 10 μM iron chloride (iron-loaded) for 24 h. Next, medium was removed, and C6 cells were rinsed and incubated in serum-free medium for 24 h. Media from the three conditions, control, iron-deficient, and iron-loaded, were collected and added to the lower chambers of the respective Transwells that have hBMVECs growing for 5–6 days as described.

Indirect Immunofluorescence—hBMVECs on coverslips were washed twice with PBS. The cells were then fixed for 10 min at room temperature with solution containing 3.7% paraformaldehyde and 4% sucrose in PBS, following previously published protocol (15). Fixing solution was removed by washing with PBS. Next, the cells were incubated for a half hour in block solution (1% BSA, 0.3 M glycine, and 0.1% Tween 20). For co-localization experiments with NHE9-GFP, primary antibodies Rab 5 (Cell Signaling Technology), Rab 11 (Cell Signaling Technology), and LBPA (Echelon) were diluted 1:100 in block solution without Tween 20 and incubated overnight at 4 °C. Following PBS washes, Alexa Fluor-conjugated secondary antibodies (Invitrogen) were used at 1:1000 dilutions for 30 min. the cells were mounted onto slides using Prolong gold antifade reagent (Invitrogen) and were imaged using Lumascope-620 microscope (Etaluma). For staining ZO1 proteins in hBMVECs cultured on Transwell filters, the cells were fixed in methanol (insert with cells were incubated in wells of ice-cold 100% methanol in 24-well tissue culture plate) at −20 °C overnight, after which they were treated with 100% acetone (−20 °C) for 1 min and were allowed to dry at 4 °C. The Transwell filter was excised and hydrated in IMF buffer (0.1% Triton X-100, 0.15 M NaCl, 5 mM EDTA, 20 mM HEPES, pH 7.5, 0.02% NaN_3 as preservative). The cells were then incubated with ZO1 antibody (Thermo Fisher Scientific) at 1:100 dilution overnight at 4 °C. The filters were then rinsed with IMF buffer and incubated with Alexa Fluor conjugated secondary antibodies (Invitrogen) at 1:1000 dilutions for 30 min and mounted as described above with Prolong gold antifade reagent (Invitrogen).

qPCR Analysis—mRNA was isolated from hBMVECs using the RNeasy mini kit (Qiagen) following the manufacturer's instructions with an additional step to remove DNA using DNase I (Ambion; Thermo Fisher Scientific). cDNA was synthesized using the high capacity RNA to cDNA kit (Applied Biosystems) following the manufacturer's instructions. Quantitative real time PCR analysis experiments were set up using TaqMan fast universal PCR Master Mix (Applied Biosystems) according to the manufacturer's instructions on CFX connect real time system (Bio-Rad). TaqMan gene expression assay probes used were: Hs02758991_g1 and Mm99999915_g1 (GAPDH), Hs00543518_m1 and Mm00626012_m (NHE9), 1Hs00951083_m1 (TfR), and Hs03003631_g1 (18S rRNA). Cycle threshold (C_t) values were first normalized to endogenous controls. Fold change was calculated as $2^{-\Delta\Delta Ct}$, where $\Delta\Delta C_t$ is the normalized cycle threshold value relative to control. Three technical replicates of three biological replicates were run to account for variance in assays.

Surface Biotinylation and Western Blotting—Cell surface proteins were labeled with biotin as previously described (27). The cells were lysed with mammalian protein extraction reagent (Thermo Fisher Scientific) that included protease inhibitor mixture (halt protease inhibitor mixture; Thermo Fisher Scientific). Lysates were centrifuged at 14,000 r.p.m. for 15 min (4 °C). Cell protein lysates (50–100 μg) were dissolved in loading buffer (62.5 mM Tris-HCl, pH 6.8, 10% glycerol, 2% SDS, 0.01% bromphenol blue, 100 mM DTT), and separated by SDS-polyacrylamide gel electrophoresis. TfR antibodies used for Western blotting were Abcam ab84036 and Thermo Fisher Scientific 13-6800 at 1:100 dilution. The loading controls used were tubulin (Sigma T 9026, 1:1000). Ferritin heavy chain antibody was a kind gift from Dr. Andrew Dancis (University of Pennsylvania).

Transferrin Efflux—For transferrin efflux experiments, hBMVECs on coverslips were rinsed and incubated in serum-free medium for 30 min. Following that, the cells were exposed to 100 μg ml^{-1} transferrin conjugated to Alexa Fluor 568 (Tfn-568) for 30 min. Dishes with coverslips were then placed on ice. After removing the medium with Tfn-568 the coverslips were rinsed twice with ice-cold PBS. The 0-min time point coverslip was fixed immediately. Other coverslips were incubated in complete medium (medium with FBS) for 10 min, rinsed, and fixed. Fluorescence images were acquired with Lumascope 620 (Etaluma), and the Tfn-568 fluorescence remaining in the cells was quantified using ImageJ (57) software.

Endosomal pH Measurement—hBMVECs plated in fluorodishes (World Precision Instruments) were placed on ice for 10 min and then rinsed with cold imaging buffer (live cell imaging solution (Thermo Fisher Scientific) with 20 mM glucose and 1% BSA) to remove residual transferrin. The cells were then incubated with 50 μg/ml fluorescein-conjugated transferrin (Tfn-FITC; Thermo Fisher Scientific) in imaging buffer for 30 min. The cells were then rinsed with live cell imaging solution, and the fluorescence images were acquired (excitation, 494 nm; and emission, 518 nm) with Lumascope 620 (Etaluma). Internal fluorescence was quantified using ImageJ (57) software, and the average fluorescence intensity was recorded. NHE9-mcherry was transfected using Lipofectamine 2000 for expression in hBMVECs. Tfn-FITC fluorescence was quantified only in mcherry-positive cells. To normalize for total transferrin uptake, pH-insensitive 50 μg/ml Alexa Fluor 568-conjugated transferrin (Tfn-568) was loaded as described above in both control and NHE9-GFP-transduced hBMVECs. Endosomal pH was determined from a standard curve that was generated using pH calibration buffer kit (Thermo Fisher Scientific). Briefly, the cells were incubated with 50 μg/ml fluorescein-conjugated transferrin for 30 min as described above and rinsed with imag-

ing buffer. The cells were then loaded with 10 μM cell loading solution (Thermo Fisher Scientific) that included valinomycin and nigericin (10 μM each) and incubated with calibration buffers of varying pH for 5 min at 37 °C, before fluorescence imaging.

Atomic Absorption Spectroscopy—hBMVECs growing on Transwells were lysed as described above using with mammalian protein extraction reagent (Thermo Fisher Scientific). Part of the lysate was diluted in 30% nitric acid, and iron levels were measured by atomic absorption spectrophotometer (Perkin-Elmer Life Sciences). Remaining lysate was used to measure total cellular protein concentrations (Thermo Fisher Scientific Pierce BCA protein assay kit). Intracellular iron levels were normalized with cellular protein concentrations. Six biological replicates were done for every condition.

Author Contributions—K. C. K. designed the research; K. C. K., R. B., M. A. H., and D. M. G. Z performed the research; K. C. K., R. B., and M. A. H. analyzed the data; and K. C. K. wrote the paper. All authors reviewed the results and approved the final version of the manuscript.

Acknowledgments—We thank Dr. Rajini Rao (Johns Hopkins University, School of Medicine), in whose laboratory NHE9-GFP and NHE9-mcherry constructs were generated. We thank Ali Abboud for assistance with one of the schematics.

References

1. Thompson, K. J., Shoham, S., and Connor, J. R. (2001) Iron and neurodegenerative disorders. *Brain Res. Bull.* **55,** 155–164
2. McCarthy, R. C., and Kosman, D. J. (2015) Mechanisms and regulation of iron trafficking across the capillary endothelial cells of the blood-brain barrier. *Front. Mol. Neurosci.* **8,** 31
3. Todorich, B., Pasquini, J. M., Garcia, C. I., Paez, P. M., and Connor, J. R. (2009) Oligodendrocytes and myelination: the role of iron. *Glia* **57,** 467–478
4. Beard, J. L., Connor, J. R., and Jones, B. C. (1993) Iron in the brain. *Nutr. Rev.* **51,** 157–170
5. Youdim, M. B. (1988) *Brain Iron: Neurochemical and Behavioural Aspects*, pp. 25–66, Taylor & Francis, New York
6. Rouault, T. A. (2013) Iron metabolism in the CNS: implications for neurodegenerative diseases. *Nat. Rev. Neurosci.* **14,** 551–564
7. McCarthy, R. C., and Kosman, D. J. (2015) Iron transport across the blood-brain barrier: development, neurovascular regulation and cerebral amyloid angiopathy. *Cell Mol. Life Sci.* **72,** 709–727
8. Ward, R. J., Zucca, F. A., Duyn, J. H., Crichton, R. R., and Zecca, L. (2014) The role of iron in brain ageing and neurodegenerative disorders. *Lancet Neurol.* **13,** 1045–1060
9. Raichle, M. E., and Gusnard, D. A. (2002) Appraising the brain's energy budget. *Proc. Natl. Acad. Sci. U.S.A.* **99,** 10237–10239
10. Duck, K. A., and Connor, J. R. (2016) Iron uptake and transport across physiological barriers. *Biometals* **29,** 573–591
11. Allen, R. P., Barker, P. B., Wehrl, F., Song, H. K., and Earley, C. J. (2001) MRI measurement of brain iron in patients with restless legs syndrome. *Neurology* **56,** 263–265
12. Abbott, N. J., Patabendige, A. A., Dolman, D. E., Yusof, S. R., and Begley, D. J. (2010) Structure and function of the blood-brain barrier. *Neurobiol. Dis.* **37,** 13–25
13. Abbott, N. J. (2002) Astrocyte-endothelial interactions and blood-brain barrier permeability. *J. Anat.* **200,** 629–638
14. Simpson, I. A., Ponnuru, P., Klinger, M. E., Myers, R. L., Devraj, K., Coe, C. L., Lubach, G. R., Carruthers, A., and Connor, J. R. (2015) A novel model for brain iron uptake: introducing the concept of regulation. *J. Cereb. Blood Flow Metab.* **35,** 48–57
15. McCarthy, R. C., and Kosman, D. J. (2014) Glial cell ceruloplasmin and hepcidin differentially regulate iron efflux from brain microvascular endothelial cells. *PLoS One* **9,** e89003
16. McCarthy, R. C., Park, Y. H., and Kosman, D. J. (2014) sAPP modulates iron efflux from brain microvascular endothelial cells by stabilizing the ferrous iron exporter ferroportin. *EMBO Rep.* **15,** 809–815
17. Casey, J. R., Grinstein, S., and Orlowski, J. (2010) Sensors and regulators of intracellular pH. *Nat. Rev. Mol. Cell Biol.* **11,** 50–61
18. Ohgaki, R., van IJzendoorn, S. C., Matsushita, M., Hoekstra, D., and Kanazawa, H. (2011) Organellar Na^+/H^+ exchangers: novel players in organelle pH regulation and their emerging functions. *Biochemistry* **50,** 443–450
19. Brett, C. L., Donowitz, M., and Rao, R. (2005) Evolutionary origins of eukaryotic sodium/proton exchangers. *Am. J. Physiol. Cell Physiol.* **288,** C223–C239
20. Kondapalli, K. C., Prasad, H., and Rao, R. (2014) An inside job: how endosomal Na^+/H^+ exchangers link to autism and neurological disease. *Front. Cell. Neurosci.* **8,** 172
21. Zhang-James, Y., DasBanerjee, T., Sagvolden, T., Middleton, F. A., and Faraone, S. V. (2011) SLC9A9 mutations, gene expression, and protein-protein interactions in rat models of attention-deficit/hyperactivity disorder. *Am. J. Med. Genet. B Neuropsychiatr. Genet.* **156B,** 835–843
22. Cardon, M., Evankovich, K. D., and Holder, J. L., Jr. (2016) Exonic deletion of SLC9A9 in autism with epilepsy. *Neurol. Genet.* **2,** e62
23. Zhao, H., Carney, K. E., Falgoust, L., Pan, J. W., Sun, D., and Zhang, Z. (2016) Emerging roles of Na^+/H^+ exchangers in epilepsy and developmental brain disorders. *Prog. Neurobiol.* **138–140**, 19–35
24. Morrow, E. M., Yoo, S. Y., Flavell, S. W., Kim, T. K., Lin, Y., Hill, R. S., Mukaddes, N. M., Balkhy, S., Gascon, G., Hashmi, A., Al-Saad, S., Ware, J., Joseph, R. M., Greenblatt, R., Gleason, D., *et al.* (2008) Identifying autism loci and genes by tracing recent shared ancestry. *Science* **321,** 218–223
25. Patak, J., Hess, J. L., Zhang-James, Y., Glatt, S. J., and Faraone, S. V. (2016) SLC9A9 Co-expression modules in autism-associated brain regions. *Autism Res.* 10.1002/aur.1670
26. Zhang-James, Y., Middleton, F. A., Sagvolden, T., and Faraone, S. V. (2012) Differential expression of SLC9A9 and interacting molecules in the hippocampus of rat models for attention deficit/hyperactivity disorder. *Dev. Neurosci.* **34,** 218–227
27. Kondapalli, K. C., Hack, A., Schushan, M., Landau, M., Ben-Tal, N., and Rao, R. (2013) Functional evaluation of autism-associated mutations in NHE9. *Nat. Commun.* **4,** 2510
28. Kondapalli, K. C., Llongueras, J. P., Capilla-González, V., Prasad, H., Hack, A., Smith, C., Guerrero-Cázares, H., Quiñones-Hinojosa, A., and Rao, R. (2015) A leak pathway for luminal protons in endosomes drives oncogenic signalling in glioblastoma. *Nat. Commun.* **6,** 6289
29. Yang, L., Faraone, S. V., and Zhang-James, Y. (2016) Autism spectrum disorder traits in Slc9a9 knock-out mice. *Am. J. Med. Genet. B Neuropsychiatr. Genet.* **171B,** 363–376
30. Meda, S. A., Narayanan, B., Liu, J., Perrone-Bizzozero, N. I., Stevens, M. C., Calhoun, V. D., Glahn, D. C., Shen, L., Risacher, S. L., Saykin, A. J., and Pearlson, G. D. (2012) A large scale multivariate parallel ICA method reveals novel imaging-genetic relationships for Alzheimer's disease in the ADNI cohort. *Neuroimage* **60,** 1608–1621
31. Martinelli-Boneschi, F., Giacalone, G., Magnani, G., Biella, G., Coppi, E., Santangelo, R., Brambilla, P., Esposito, F., Lupoli, S., Clerici, F., Benussi, L., Ghidoni, R., Galimberti, D., Squitti, R., Confaloni, A., *et al.* (2013) Pharmacogenomics in Alzheimer's disease: a genome-wide association study of response to cholinesterase inhibitors. *Neurobiol. Aging* **34,** 1711.e7–1711.e13
32. Coelho, L., Goertzel, B., Pennachin, C., and Heward, C. (2010) Classifier ensemble based analysis of a genome-wide SNP dataset concerning late-onset Alzheimer disease. *Int. J. Software Sci. Comput. Intelligence*, 10.1109/COGINF.2009.5250695
33. Pérez-Palma, E., Bustos, B. I., Villamán, C. F., Alarcón, M. A., Avila, M. E., Ugarte, G. D., Reyes, A. E., Opazo, C., De Ferrari, G. V., Alzheimer's Disease Neuroimaging Initiative, and NIA-LOAD/NCRAD Family Study

Group (2014) Overrepresentation of glutamate signaling in Alzheimer's disease: network-based pathway enrichment using meta-analysis of genome-wide association studies. *PLoS One* **9,** e95413
34. Zecca, L., Youdim, M. B., Riederer, P., Connor, J. R., and Crichton, R. R. (2004) Iron, brain ageing and neurodegenerative disorders. *Nat. Rev. Neurosci.* **5,** 863–873
35. Drayer, B., Burger, P., Darwin, R., Riederer, S., Herfkens, R., and Johnson, G. A. (1986) MRI of brain iron. *AJR Am. J. Roentgenol.* **147,** 103–110
36. Connor, J. R., Menzies, S. L., St Martin, S. M., and Mufson, E. J. (1990) Cellular distribution of transferrin, ferritin, and iron in normal and aged human brains. *J. Neurosci. Res.* **27,** 595–611
37. Hill, J. M., and Switzer, R. C., 3rd (1984) The regional distribution and cellular localization of iron in the rat brain. *Neuroscience* **11,** 595–603
38. *Allen Human Brain Atlas* (2010) Allen Institute for Brain Science, Seattle, WA
39. Demeuse, P., Kerkhofs, A., Struys-Ponsar, C., Knoops, B., Remacle, C., and van den Bosch de Aguilar, P. (2002) Compartmentalized coculture of rat brain endothelial cells and astrocytes: a syngenic model to study the blood-brain barrier. *J. Neurosci. Methods* **121,** 21–31
40. Boveri, M., Berezowski, V., Price, A., Slupek, S., Lenfant, A. M., Benaud, C., Hartung, T., Cecchelli, R., Prieto, P., and Dehouck, M. P. (2005) Induction of blood-brain barrier properties in cultured brain capillary endothelial cells: comparison between primary glial cells and C6 cell line. *Glia* **51,** 187–198
41. Gaillard, P. J., Voorwinden, L. H., Nielsen, J. L., Ivanov, A., Atsumi, R., Engman, H., Ringbom, C., de Boer, A. G., and Breimer, D. D. (2001) Establishment and functional characterization of an *in vitro* model of the blood-brain barrier, comprising a co-culture of brain capillary endothelial cells and astrocytes. *Eur. J. Pharm. Sci.* **12,** 215–222
42. Easton, A. S., and Abbott, N. J. (2002) Bradykinin increases permeability by calcium and 5-lipoxygenase in the ECV304/C6 cell culture model of the blood-brain barrier. *Brain Res.* **953,** 157–169
43. Hurst, R. D., and Fritz, I. B. (1996) Properties of an immortalised vascular endothelial/glioma cell co-culture model of the blood-brain barrier. *J. Cell. Physiol.* **167,** 81–88
44. Díaz-Coránguez, M., Segovia, J., López-Ornelas, A., Puerta-Guardo, H., Ludert, J., Chávez, B., Meraz-Cruz, N., and González-Mariscal, L. (2013) Transmigration of neural stem cells across the blood brain barrier induced by glioma cells. *PLoS One* **8,** e60655
45. Theil, E. C. (1990) Regulation of ferritin and transferrin receptor mRNAs. *J. Biol. Chem.* **265,** 4771–4774
46. Nakamura, N., Tanaka, S., Teko, Y., Mitsui, K., and Kanazawa, H. (2005) Four Na^+/H^+ exchanger isoforms are distributed to Golgi and post-Golgi compartments and are involved in organelle pH regulation. *J. Biol. Chem.* **280,** 1561–1572
47. Donowitz, M., Ming Tse, C., and Fuster, D. (2013) SLC9/NHE gene family, a plasma membrane and organellar family of Na^+/H^+ exchangers. *Mol. Aspects Med.* **34,** 236–251
48. McCarthy, R. C., and Kosman, D. J. (2012) Mechanistic analysis of iron accumulation by endothelial cells of the BBB. *Biometals* **25,** 665–675
49. Connor, J. R., Ponnuru, P., Wang, X. S., Patton, S. M., Allen, R. P., and Earley, C. J. (2011) Profile of altered brain iron acquisition in restless legs syndrome. *Brain* **134,** 959–968
50. Cabantchik, Z. I. (2014) Labile iron in cells and body fluids: physiology, pathology, and pharmacology. *Front. Pharmacol.* **5,** 45
51. Du, F., Qian, Z. M., Luo, Q., Yung, W. H., and Ke, Y. (2015) Hepcidin suppresses brain iron accumulation by downregulating iron transport proteins in iron-overloaded rats. *Mol. Neurobiol.* **52,** 101–114
52. Gunshin, H., Mackenzie, B., Berger, U. V., Gunshin, Y., Romero, M. F., Boron, W. F., Nussberger, S., Gollan, J. L., and Hediger, M. A. (1997) Cloning and characterization of a mammalian proton-coupled metal-ion transporter. *Nature* **388,** 482–488
53. Levy, A. F., Zayats, M., Guerrero-Cazares, H., Quiñones-Hinojosa, A., and Searson, P. C. (2014) Influence of basement membrane proteins and endothelial cell-derived factors on the morphology of human fetal-derived astrocytes in 2D. *PLoS One* **9,** e92165
54. Nizet, V., Kim, K. S., Stins, M., Jonas, M., Chi, E. Y., Nguyen, D., and Rubens, C. E. (1997) Invasion of brain microvascular endothelial cells by group B streptococci. *Infect. Immun.* **65,** 5074–5081
55. D'Sa, C., Hirayama, K., West, A., Hahn, M., Zhu, M., and Kapatos, G. (1996) Tetrahydrobiopterin biosynthesis in C6 glioma cells: induction of GTP cyclohydrolase I gene expression by lipopolysaccharide and cytokine treatment. *Brain Res. Mol. Brain Res.* **41,** 105–110
56. Li, G., Simon, M. J., Cancel, L. M., Shi, Z. D., Ji, X., Tarbell, J. M., Morrison B., 3rd, Fu, B. M. (2010) Permeability of endothelial and astrocyte cocultures: *in vitro* blood-brain barrier models for drug delivery studies. *Ann. Biomed. Eng.* **38,** 2499–2511
57. Schneider, C. A., Rasband, W. S., and Eliceiri, K. W. (2012) NIH Image to ImageJ: 25 years of image analysis. *Nat. Methods* **9,** 671–675